Use of an integrated approach to characterize the physicochemical properties of foundry green sands

Raquel L.P. Carnin[a], Marilena Valadares Folgueras[b], Rúbia Raquel Luvizão[b], Sivaldo Leite Correia[b], Carlos Jorge da Cunha[c], Robert S. Dungan[d],*

[a] Tupy S.A., Rua Albano Schmidt 3.400, Joinville, Santa Catarina, Brazil
[b] Universidade do Estado de Santa Catarina, Rua Paulo Malschitzki, s/numero – Campus Universitário Prof. Avelino Marcante, Bairro Zona Industrial Norte, Joinville, Santa Catarina, Brazil
[c] Universidade Federal do Paraná, Centro Politécnico, Jardim das Américas, Curitiba, Paraná, Brazil
[d] USDA-ARS, Northwest Irrigation & Soils Research Laboratory, 3793 North 3600 East, Kimberly, ID 83341, USA

ABSTRACT

A fresh green sand, spent green sand, and a weathered spent green sand (wSGS) from a foundry landfill were analyzed using diffractometry, electron microscopy, fluorometry, granulometry, spectrometry, and thermogravimetry (TG). Our objective was to understand how the physicochemical properties of the foundry green sands change from their original form after being subjected to the casting process, then after weathering at the landfill. A quantitative phase composition model was also postulated for each material based on the TG results and it was found to be the most reliable and informative quantitative data for this type of residue. The weathered sample, that remained in a landfill for two years, was found to be composed of almost pure sand. Because of the weathering process, it may be possible to use the wSGS as a virgin sand replacement in the regeneration system or in geotechnical applications where bentonite would affect the properties of the final product.

Published by Elsevier B.V.

1. Introduction

Sands are used worldwide by the foundry industry to create molds and cores for metalcasting processes. The world foundry sector generates some 100 million tons of spent foundry sand (SFS) annually, while in Brazil it is estimated that 3 million tons are generated. The majority of SFSs are green sands, which use clays (e.g. bentonite, kaolinite) as the sand bonding agent [1]. According to Brazilian standards, spent green sands (SGSs) are classified as a non-inert residue due to the potential leaching of toxic metal ions [2]. Recent research, however, has demonstrated that the majority of SGSs and other foundry sands possess metal and organic concentrations similar to those found in native soils and are not hazardous in nature [3–6].

Because iron foundries produce the largest portion of the total casting volume when compared to other ferrous and non-ferrous foundries, there is concern over the large quantities of SGS generated by these facilities. While some foundries have private on-site landfills, the disposal of spent sands in controlled landfills can place an economic burden upon some foundries due to high tipping fees.

In an effort to reduce disposal costs, maximize the life expectancy of landfills and minimize environmental impacts associated with the mining of virgin sands, geotechnical and agricultural uses for SFSs are being sought [7,8]. To date, SFSs have been successfully been used as aggregate replacement in asphalt [9,10], highway subbases [11], ceramic materials [12,13], manufactured soils [8,14], retaining walls [15], concrete [16,17], highway embankments [18], controlled low-strength materials [19,20], and flowable slurry [21,22].

To characterize the physicochemical properties of SFSs, a variety of techniques have been applied, such as near- and mid-infrared spectroscopy [23,24], thermogravimetry (TG) [25], pyrolysis gas chromatography–mass spectrometry [26], X-ray diffraction (XRD) and scanning electron microscopy (SEM) [27]. These techniques were utilized to assess the suitability of using SFSs in various beneficial use applications, with specific concerns about the presence of organic contaminants and the potential of the sands to impede root growth in soil blends. This integrated approach has also been applied to various types of industrial residues, including byproducts from a paper mill and electric arc furnace dusts [28,29].

In this study, a fresh green sand (FGS), SGS, and a weathered spent green sand (wSGS) from a landfill were obtained from an iron foundry in the state of Santa Catarina, Brazil, and analyzed using granulometry, FTIR spectrometry, SEM, TG, XRD, and X-ray fluorometry (XRF). Our objective was to understand how the

physicochemical properties of the green sands change from their original form after being subjected to the casting process, then after weathering at the landfill. It was also hoped that this integrated approach could be used to determine the suitability of using SFSs for beneficial use applications. While the iron foundry currently uses SGS to manufacture interlocking pavement [30], there is interest in using both SGS and wSGS as aggregate in hot mix asphalt. Recovery and beneficial use of sands from the landfill is of particular interest, as it would be helpful in extending the landfill's useful life.

2. Materials and methods

2.1. Description of the iron foundry

The iron foundry was located in the state of Santa Catarina in southern Brazil. Scrap iron, pig iron, spent steel shot, iron silicon alloy (rarely used), silicon carbide, coke, and limestone are processed in a cupola furnace that produces 21.5 metric tons of metal per hour. The molten metal with the desired composition is poured into green sand molds at around 1400 °C. After solidification and cooling to 630 °C, the molds are sent to a casting shakeout belt to promote the disaggregation of the molds. After shakeout, the green sands and core butts are manually disaggregated, then sent to the muller for regeneration. While most of the green sands are reclaimed, about 15% are discarded and new components are added to make up for the sand removed. New sands are added to maintain the engineering specifications of the molding sands and replace sand lost during the casting process. The green sands contain 91.3% silica sand, 7.3% bentonite clay, 1.4% seacoal, and 1.8% water (w/w) prior to casting. Each year the foundry generates about 400,000 metric tons of SGS.

2.2. Preparation of the fresh green sand

Fresh green sand was prepared in the laboratory using 4200 g of silica sand, 168 g of natural sodium bentonite, 168 g of sodium-activated bentonite, 63 g of seacoal (i.e. pulverized bituminous coal), and 84 mL of deionized water. The materials were mixed in a laboratory-size muller for about 1.5 min and then allowed to cool to room temperature. As with all green sands, the addition of seacoal to the mixture causes it to be black in color.

2.3. Collection of the spent and weathered green sands

About 2 kg of SGS was collected at the point of disposal in the foundry, which was then divided into 15 g quantities using a riffle splitter. Because the green sands are produced in a highly controlled environment, it is expected that the grab sample composition was similar to the bulk quantity of SGS produced.

Weathered SGS was collected at an on-site landfill at the foundry, which has been receiving sand waste for seven years. The sand samples, which were estimated to be two years old, were collected from the surface of the landfill where it was exposed to rain and temperature fluctuations. The wSGS was collected to a depth of 39 cm in the landfill using a sampling trier as specified by method NBR 10.007 [2]. After that, the samples were placed into clean plastic bags, then transferred to the laboratory for subsequent analysis.

2.4. Analysis of the green sands

All green sand samples were dried at 70 °C for 48 h prior to analysis, unless specified otherwise.

The XRF measurements were performed using a Philips PW 2400 X-ray spectrometer. Each dry, non-ground, sample was mixed with wax and pressed to form a pellet. The results were interpreted with

Table 1
Composition (mass%) of the FGS, SGS, and wSGS as determined by XRF.

Element	FGS	SGS	wSGS
Al	5.61	4.21	0.83
Ba	0.10	0.11	0.00
Ca	0.53	1.00	0.10
Cl	0.27	0.65	0.00
Fe	1.95	2.82	0.57
K	0.89	0.93	0.36
Mg	0.73	0.30	0.00
Mn	0.04	0.00	0.00
Na	0.69	0.27	0.00
P	0.04	0.63	0.00
S	0.44	0.95	0.02
Si	29.8	29.0	36.4
Sr	0.15	0.15	0.00
Ti	0.43	0.46	0.06
Zr	0.00	0.04	0.99
O (fixed oxides)[a]	55.7	54.9	59.9
Loss on ignition	2.67	3.64	0.77
Total	100	100	100

[a] Oxygen present in the fixed oxides estimated from the oxide of each element. It does not account for the oxygen of water lost on dehydroxylation, nor for the oxygen present in seacoal that was lost during combustion.

the Philips Semi-Q software and normalized to 100%. This normalization takes into account the loss on ignition (LOI) estimated as the total mass loss of the dried material, between 200 and 800 °C, measured in the TG experiment.

For the XRD analysis, each sample was manually ground to produce a powder suitable for the experiment. The diffractometer used was a Shimadzu LabX XRD-6000 (radiation Cu Kα, θ/2θ scans, 40 kV and 30 mA). The diffractograms were interpreted with the aid of the following data banks: ICDD [31], MINCRYST [32], and Webmineral [33].

Simultaneous TG and differential thermal analysis (DTA) were conducted on a Netzsch STA 449C thermal analyzer. A dry sample, weighing between 20 and 35 mg, was placed in an aluminum crucible and heated, under a synthetic air flux of 70 mL min^{-1}, from room temperature up to 800 °C at a rate of 10 °C min^{-1}.

Fourier transform infrared spectra were collected for FGS, SGS, seacoal, natural bentonite, and activated bentonite using a Bomem MB-100 FTIR spectrometer, in KBr pellets, between 4000 and 400 cm^{-1} with a 4 cm^{-1} resolution and 32 scans.

For SEM, each sample was dried for 24 h at 100 °C, then glued to a carbon conducting tape that was fixed to an aluminum holder, which was then metalized with gold under an argon atmosphere. The surface, so prepared, was observed with a Zeiss DSM 940 SEM with an energy dispersive X-ray spectrometer.

The particle size analysis was performed according to DNER method ME 083/98 [34] by loading 1 kg of dry sample into a sieve shaker with a series of five sieves of the following sizes: 4.8, 2.0, 0.42, 0.18, and 0.074 mm. The shaking time was 10 min. The textural class was determined using the USDA soil textural triangle [35]. The pH of each sample was determined according to SW-846 method 9045D [36].

3. Results and discussion

3.1. Elemental analysis

The elemental composition of the green sand samples, as determined by XRF, is presented in Table 1. Since these analyses were conducted on non-ground samples, the measured concentrations could potentially be overestimated when compared to those of ground samples, as the elements may be enriched at the surface of the sand grains. Conversely, if the elements were enriched within the silica sand matrix, then the concentrations could be

Table 2
Values (mass%) for loss on ignition, organic matter content, and dehydroxylation in the FGS, SGS, and wSGS.[a]

	FGS	SGS	wSGS
Loss on ignition	2.67	3.64	0.77
OM content	1.59 (2[a])	2.61 (2)	0.77 (2)
Dehydroxylation	1.08 (3)	1.03 (3)	–

[a] Numbers in parentheses correspond to the thermal events identified in the DTA curves in Fig. 1.

underestimated when compared to ground samples. Because the sand grains were covered with sodium bentonite (aluminum phyllosilicate) and seacoal, it is likely that elements such as Al, Ca, Mg, Na, O, and Si were overestimated.

When comparing the elemental composition between the FGS and SGS, the SGS contains less Al, Mg and Na, which can be attributed to the high casting temperature and partial loss of bentonite clays during disaggregation of the used molds. In contrast, the Fe content was slightly greater in the SGS (2.8%) than in the FGS (2.0%) due to the incorporation of iron during the casting process and dry deposition of Fe-containing dust. The elements Ca, Cl, P, and S were also greater in the SGS than in the FGS due to the accumulation of salts present in the treated water supplied by the local water utility. Green sand molds at the foundry contain 1.8% water (w/w) prior to casting.

Aside from O, the other most abundant element was Si at about 30% in the FGS and SGS and 36% in the wSGS and this is largely a result of silica sand (SiO_2) being used, although Si is also present in the bentonite clay. Because the values in Table 1 are presented on a mass% basis, the greater Si content in the wSGS can be attributed to the loss of most elements during weathering in the landfill. Due to abundant rainfall in the region of the foundry (annual average of 170 cm), it is expected that leaching is the dominant weathering process. The fact that the wSGS is predominantly composed of Si and O, suggests that most of the bentonite clay and seacoal has been removed from the sand's surface.

The pH of the FGS and SGS was 8.66 and 7.98, respectively. The alkaline character of these sands originates from the presence of sodium-activated bentonite. Calcium bentonites are often activated using sodium bicarbonate to produce sodium bentonites, which are more durable and have a higher green strength [37]. The SGS pH was slightly lower than that of the FGS, which could be due to the presence of acidic cations (e.g. Fe^{2+}) that undergo hydrolysis. Compared to the FGS and SGS, the pH of the wSGS was lower at 6.97, which suggests that the sand contained fewer acidic cations and activated bentonite.

3.2. X-ray diffraction

The diffractograms from the FGS, SGS and wSGS were very similar since the major component of the samples was α quartz. Despite the high temperatures used during casting, the sand was not found to undergo thermal conversion to β quartz. Diffraction peaks, characteristic of bituminous coal and bentonite clay, could not be identified in any of these three diffractograms (data not shown).

3.3. Thermal analysis

Thermogravimetric and DTA curves for the FGS, SGS, and wSGS under a synthetic air atmosphere are presented in Fig. 1. Because the samples lost moisture from room temperature up to around 150 °C, the sample mass was set to 100% (dry weight basis) at 200 °C. The LOI, as determined from the mass lost during heating from 200 to 800 °C, was ≤3.6% for all samples (Table 2). The
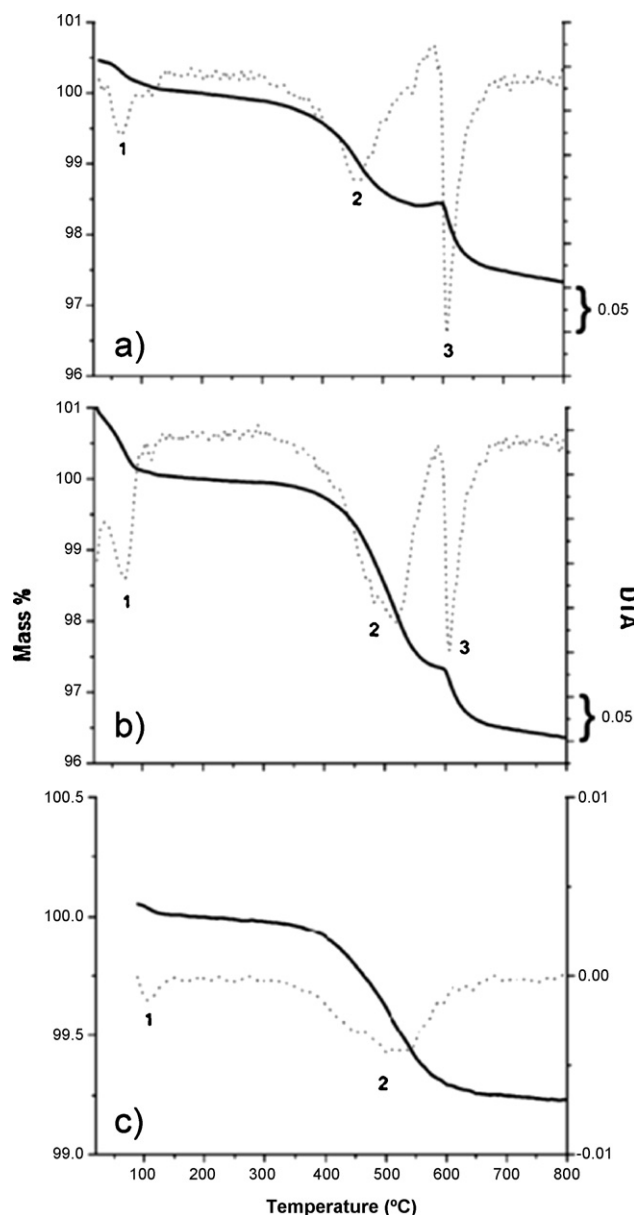

Fig. 1. Thermogravimetric and DTA curves for (a) FGS, (b) SGS, and (c) wSGS under a synthetic air flux and heating of 10 °C min⁻¹. Peaks 1, 2, and 3 are due to loss of moisture, thermal decomposition of seacoal, and dehydroxylation of bentonite, respectively.

thermal processes, as numerically assigned in Fig. 1, were identified by comparing TG data from the green sand samples and raw materials (i.e. bentonite and seacoal). Peaks 1, 2, and 3 correspond to the loss of moisture, thermal decomposition of seacoal, and dehydroxylation of bentonite clay, respectively. Similar TG results from foundry sands were obtained by Cannon and Voigt [38] and Dungan and Reeves [25]. By comparing the LOI values between the SGS and wSGS (Table 2), it was estimated that the wSGS contains 79% less bentonite and seacoal than the SGS. This represents an approximate estimate of materials removed from the sand grains due to weathering.

3.4. FTIR spectroscopy

The infrared spectra of the foundry sands and raw materials are presented in Fig. 2. The spectra of FGS and SGS are very similar, as both closely resemble the sand spectrum with a band
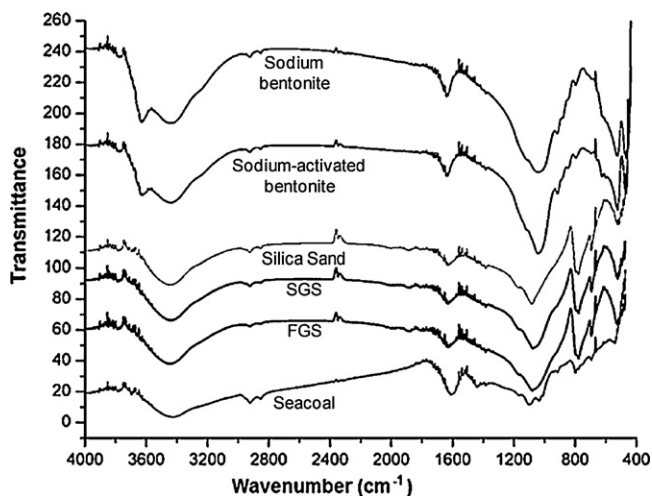
Fig. 2. Infrared spectra of FGS, SGS and raw materials prepared as KBr pellets.

Table 4
Estimated mineral phase composition (mass%) of the FGS, SGS, and wSGS based on mass lost during thermal analysis.

Component	FGS	SGS	wSGS	Green sand[a]
Sand (α quartz)	90.5	89.7	99.1	91.3
Bentonite clay	7.7	7.4	0	7.3
Seacoal	1.8	2.9	0.9	1.4
Total	100	100	100	100

[a] Composition based on the actual green sand formula used by the foundry, not mass lost during thermal analysis.

around 1070 cm^{-1}, which is broadened due to the overlap with the 1031 cm^{-1} band of the bentonite clays. The seacoal also has an overlapping band in this region (i.e. 1040 cm^{-1}). The O—H stretch band, located at 3632 cm^{-1} in the spectra of both bentonite clays [39], was not seen in the FGS nor in the SGS spectra. This is likely due to the fact that the green sands were only prepared with about 7% bentonite clay. The bands around 3450 and 1633 cm^{-1} indicate the presence of water in all materials. The Si—O band around 518 cm^{-1} was present in all of the Si-containing materials (i.e. bentonite, silica sand), except the seacoal. The characteristic quartz bands at 784 and 690 cm^{-1} are seen in the sand, as well as in the FGS and SGS spectra. The carbonate band expected at 1440 cm^{-1} was not seen in the activated bentonite, indicating that sodium carbonate does not heavily contaminate the bentonite. The seacoal has bands characteristic of carbonate vibrations at 1440 and 1040 cm^{-1}, but these were not visible in the FGS and SGS spectra.

3.5. Granulometric analysis

The results for the particle-size distribution of the FGS, SGS and wSGS are presented in Table 3. While the results are somewhat similar, the biggest difference between the sands is that the SGS contains a larger mass fraction (i.e. 8.7%) of particles <0.074 mm in diameter. The absence of these smaller particles in the wSGS once again indicates that the weathering process may be responsible. Interestingly, the amount of seacoal and bentonite added to the FGS was 8.7% (Table 4), which is the same mass% determined for particles <0.074 mm in the SGS. These almost identical values suggest that the finer fraction of the SGS corresponds to seacoal and bentonite, with this fraction being absent in the wSGS. In contrast, however, particles <0.074 mm in the FGS only accounted for 2% of

Table 3
Particle size distribution of FGS, SGS, and wSGS obtained using a dry sieve method.

Particle size (mm)	Mass%		
	FGS	SGS	wSGS
>4.8	0	0	0
4.8–2.0	0	0	0.8
2.0–0.42	17.6	21.4	29.3
0.42–0.18	67.0	51.6	52.8
0.18–0.074	13.4	18.3	17.1
<0.074	2.0	8.7	0
Total	100	100	100

the total mass. This could be a result of limitations associated with the dry sieving method.

Based upon the information in Table 3, the estimated texture class of the FGS, SGS and wSGS is sand. This result is similar to that of Dayton and coworkers [14], who determined that the texture of SFSs ranged from a sand to a sandy loam.

3.6. Scanning electron microscopy

Scanning electron microscopic images of the FGS, SGS and wSGS are presented in Fig. 3. The image of the FGS (Fig. 3a) shows that there is a complete coating of bentonite and seacoal over the surface of the sand grain, which is accomplished through the use of mullers. However, after the sands have been exposed to temperatures as high as 1400 °C during the casting process, it is evident that the bentonite/seacoal coating has been disturbed (Fig. 3b). This likely occurs due to dehydration and dehydroxylation of the clays, while the seacoal undergoes thermal decomposition. Additionally, it is also possible that the coating was disturbed as a result of abrasion of sand grains during the breaking of molds and recovery of the sands. Dehydration and dehydroxylation of bentonite are endothermic processes and correspond to a mass loss [40]. Seacoal and other organic additives undergo thermal decomposition within the molds, resulting in the formation of volatile compounds [25]. In the case of the wSGS, the grains appear to be devoid of bentonite and seacoal after two years of storage in the landfill (Fig. 3c). As previously mentioned, the high rainfall in the region is likely responsible for the removal of the coating. However, since the wSGS was collected from the near surface, we are not certain as to whether this process also occurs deeper within the landfill.

3.7. Mineral phase quantification

Utilizing the TG data only, a phase composition model was established for the FGS, SGS, and wSGS (Table 4). While phase quantification can also be performed using XRD data if suitable standards are available, in this study it was not possible because only α quartz was visible in the X-ray diffractograms. To estimate the mineral phases within the FGS, SGS, and wSGS, the following assumptions were employed: (i) amount of seacoal was determined from the mass loss that occurred during thermal decomposition of organic matter (i.e. peak 2, Fig. 1); (ii) amount of bentonite determined from mass loss during hydroxylation (i.e. peak 3, Fig. 1); and (iii) amount of α quartz determined by subtracting the estimated bentonite and seacoal values from the total mass determined at 200 °C. Compared to the actual green sand formula, the use of TG was quite effective in estimating the actual mineral phase composition of the FGS, although it slightly overestimated the bentonite and seacoal mass. Interestingly, the total mass of seacoal was determined to be 2.93% in the SGS, as compared to 1.79% in the FGS. Since the seacoal undergoes thermal decomposition during casting, the mass should theoretically be lower in the SGS. The fact that the estimated seacoal mass is higher in the SGS is likely a result of seacoal and other organic materials (e.g. core resins) building up molding sand during reclamation and reuse. The wSGS is assumed to be made of almost
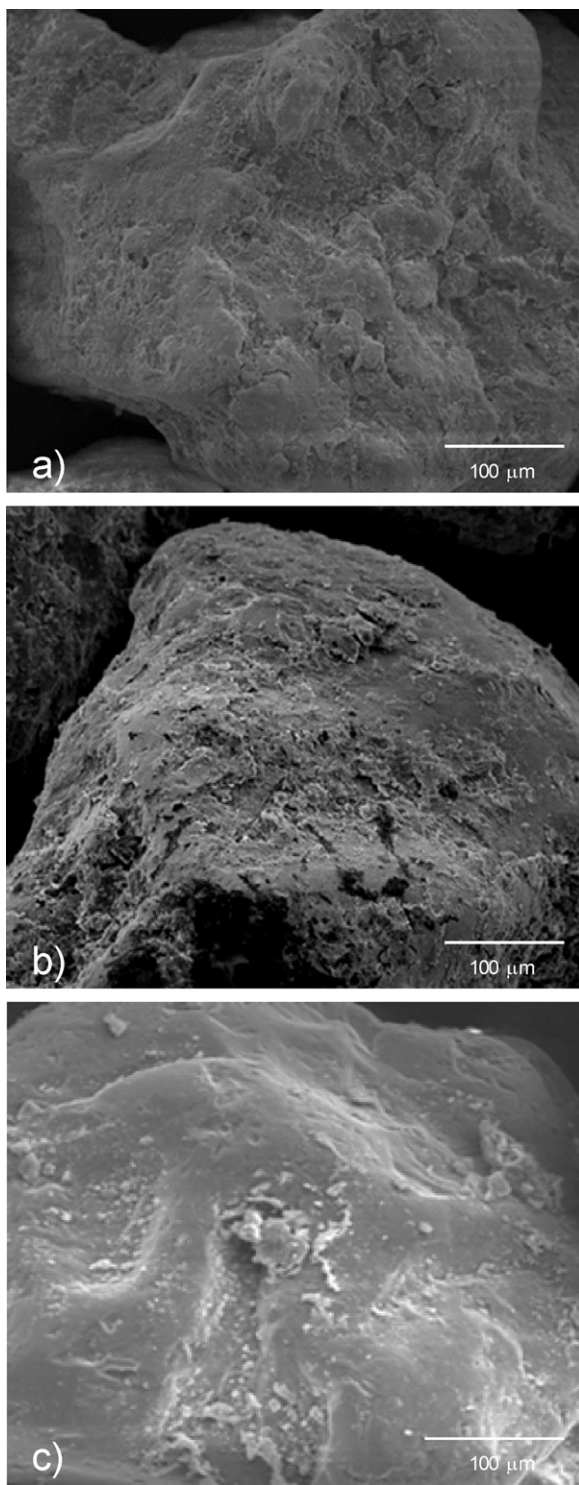
Fig. 3. Scanning electron microscopic images of (a) FGS, (b) SGS, and (c) wSGS.

pure sand since its LOI was negligible, which was also confirmed by the SEM images.

4. Conclusion

Looking at all data generated, it can be concluded that the TG analysis was the most informative technique to characterize the green sand samples. From a single TG run and simple calculations performed on the results, one can determine the % moisture, and mass of seacoal, bentonite, and quartz. One striking chemical

difference between the sand samples was that the SGS contained more Ca, Cl, P, and S than the FGS, suggesting that salts present in the treated water were accumulating in the reclaimed sands. While not expected, the SGS also contained a greater amount of seacoal, which is likely due to a buildup of seacoal during regeneration of the system sand. In contrast, the wSGS was largely devoid of bentonite and seacoal and this can be attributed to percolation of water through the landfill. The action of microorganisms on the sand coating should also not be ruled out, since the topmost part of the landfill was covered with vegetation. Because of the weathering process, it may be possible to use the wSGS as a virgin sand replacement in the regeneration system or in geotechnical applications where bentonite would affect the properties of the final product.

Acknowledgments

References

[1] T. Cobett, The ABCs of green sand, Foundry Manage. Technol. April (2002) 24.
[2] Associação Brasileira de Normas Técnicas (ABNT), NBR 10.004, Resíduos Sólidos–Classificação. Available at http://www.abnt.org.br (accessed on 17.01.2012), 2004.
[3] A. Deng, Contaminants in waste foundry sands and its leachate, Int. J. Environ. Pollut. 38 (2009) 425–443.
[4] R.S. Dungan, N.H. Dees, The characterization of total and leachable metals in foundry molding sands, J. Environ. Manage. 90 (2009) 539–548.
[5] R.S. Dungan, J. Huwe, R.L. Chaney, Concentrations of PCDD/PCDFs and PCBs in spent foundry sands, Chemosphere 75 (2009) 1232–1235.
[6] R. Siddique, G. Kaur, A. Rajor, Waste foundry sand and its leachate characteristics, Res. Conserv. Recycl. 54 (2010) 1027–1036.
[7] D.S. Leidel, M. Novakowski, D. Pohlman, Z.D. MacRunnels, M.H. MacKay, External beneficial reuse of spent foundry sand, AFS Trans. 102 (1994) 235–243.
[8] B.J. Lindsay, T.J. Logan, Agricultural reuse of foundry sand, J. Resid. Sci. Technol. 2 (2005) 3–12.
[9] K.P. Delage, A. Braham, H.U. Bahia, P. Romero, T.P. Harman, Performance testing of hot mix asphalt produced with recycled foundry sand, in: 80th Annual Meeting of the Transportation Research Board, 2001 (Paper No. 01-2844).
[10] R. Bakis, H. Koyuncu, A. Demirbas, An investigation of waste foundry sand in asphalt concrete mixtures, J. Waste Manage. Res. 24 (2006) 269–274.
[11] Y. Guney, A.H. Aydilek, M.M. Demirkan, Geoenvironmental behavior of foundry sand amended mixtures for highway subbases, J. Waste Manage. Res. 26 (2006) 932–945.
[12] S.R. Braganca, J. Vicenzi, K. Guerino, C.P. Bergmann, Recycling of iron foundry sand and glass waste as raw material for production of whiteware, J. Waste Manage. Res. 24 (2006) 60–66.
[13] S.W. Rhee, W.K. Lee, Characteristics of spent foundry sand–loess mixture as ceramic support materials, Mater. Sci. Forum 510-511 (2006) 378–381.
[14] E.A. Dayton, S.D. Whitacre, R.S. Dungan, N.T. Basta, Characterization of physical and chemical properties of spent foundry sands pertinent to beneficial use in manufactures soils, Plant Soil 329 (2010) 27–33.
[15] K.H. Lee, J.Y. Cho, R. Salgado, I. Lee, Retaining wall model test with waste foundry sand mixture backfill, Geotech. Testing J. 24 (2001) 401–408.
[16] R. Siddique, G. de Schutter, A. Noumowe, Effect of used-foundry sand on the mechanical properties of concrete, Construct. Build. Mater. 23 (2009) 976–980.
[17] G. Singh, R. Siddique, Abrasion resistance and strength properties of concrete containing waste foundry sand (WFS), Construct. Build. Mater. 28 (2012) 421–426.
[18] B.K. Partridge, J.E. Alleman, P.J. Fox, D.G. Mast, Performance evaluation of highway embankment constructed with waste foundry sand, J. Trans. Res. Board 1619 (1998) 55–63.
[19] R. Siddique, A. Noumowe, Utilization of spent foundry sand in controlled low-strength materials and concrete, Res. Conserv. Recycl. 53 (2008) 27–35.
[20] P. Tikalsky, M. Gaffney, R. Regan, Properties of controlled low-strength material containing foundry sand, ACI Mater. J. 97 (2000) 698–702.
[21] A. Deng, P.J. Tikalsky, Geotechnical and leaching properties of flowable fill incorporating waste foundry sand, Waste Manage. 28 (2008) 2161–2170.
[22] T.R. Naik, S.S. Singh, Permeability of flowable slurry materials containing foundry sand and fly ash, J. Geotech. Geoenviron. Eng. 123 (1997) 446–452.
[23] R.S. Dungan, J.B. Reeves III, Mid-infrared spectroscopic analysis of foundry green sands and chemically bonded cores, J. Resid. Sci. Technol. 3 (2006) 61–66.
[24] R.S. Dungan, J.B. Reeves III, Near infrared reflectance spectroscopic analysis of foundry sands, J. Near Infrared. Spectrosc. 115 (2007) 189–194.
[25] R.S. Dungan, J.B. Reeves III, Pyrolysis of carbonaceous foundry sand additives: seacoal and gilsonite, Thermochim. Acta 460 (2007) 60–66.

[26] Y. Wang, H. Huang, F. Cannon, R.C. Voigt, S. Komarneni, J.C. Furness, Evaluation of volatile hydrocarbon emission characteristics of carbonaceous additives in green sand foundries, Environ. Sci. Technol. 41 (2007) 2957–2963.

[27] J.P. de Koff, B.D. Lee, R.S. Dungan, Amelioration of physical strength in waste foundry green sands for reuse as a soil amendment, J. Environ. Qual. 37 (2008) 2332–2338.

[28] F.M. Martins, J.M. Martins, L.C. Ferracin, C.J. da Cunha, Mineral phases of green liquor dregs, slaker grits, lime mud and wood ash of a Kraft pulp and paper mill, J. Hazard. Mater. 147 (2007) 610–617.

[29] F.M. Martins, J.M.R. Neto, C.J. da Cunha, Mineral phases of weathered and recent electric arc furnace dust, J. Hazard. Mater. 154 (2008) 417–425.

[30] R.L.P. Carnin, C.O. Silva, R.J. Pozzi, M.V. Folgueras, W. Malkowski, Desenvolvimento de peças de concreto (Paver) contendo areia descartada de fundição para pavimento intertravado, Revista Pavimentação, 2010.

[31] International Center for Diffraction Data (ICDD). Available at http://www.icdd.com (accessed on 17.01.12).

[32] MINCRYST, Crystallographic and crystallochemical database for minerals and their structural analogues. Available at http://database.iem.ac.ru/mincryst/index.php (accessed on 17.01.12).

[33] Webmineral Mineralogy database. Available at http://www.webmineral.com (accessed on 17.01.12).

[34] Departamento Nacional de Estradas de Rodagem (DNER), Ministério dos Transportes, Brasil, ME 083/98 Agregados-Análise Granulométrica, Rio de Janeiro, 1998, p. 3.

[35] USDA., Soil Survey Manual, United States Department of Agriculture, Handbook No. 18, U.S. Government Printing Office, Washington, DC, 2003.

[36] U.S. EPA, Soil and waste pH, method 9045D. SW-846 On-line. Available at http://www.epa.gov/osw/hazard/testmethods/sw846/pdfs/9045d.pdf, 2004.

[37] F. Boylu, Optimization of foundry sand characteristics of soda-activated calcium bentonite, Appl. Clay Sci. 52 (2011) 104–108.

[38] F.S. Cannon, R.C. Voigt, Non-incineration treatment to reduce benzene and VOC emissions from greensand systems, Final report to the U.S. Department of Energy, DE-FC0799ID13719, 2002.

[39] M.J. Wilson, Clay Mineralogy: Spectroscopic and Chemical Determinative Methods, 1st edition, Chapman & Hall, London, England, 1994.

[40] M. Holtzer, A. Bobrowski, S. Żymankowska-Kumon, Temperature influence on structural changes of foundry bentonites, J. Mol. Struct. 1004 (2011) 102–108.